sustainability

MDPI

Article

Spatiotemporal Analysis of Urban Thermal Effects Caused by Heat Waves through Remote Sensing

David Hidalgo García *, Julián Arco Díaz, Adelaida Martín Martín and Emilio Gómez Cobos

Department of Architectural Graphic Expression, Technical Superior School of Building Engineering, University of Granada, 18071 Granada, Spain
* Correspondence: dhidalgo@ugr.es

Abstract: In recent years there has been an increase in the number of extreme weather events that lead to higher mortality, such as heat waves. This study carries out a new investigation that integrates the environmental quality parameters—the Surface Urban Heat Island (SUHI) and the Terrestrial Surface Temperature (LST)—during these periods of high temperatures and compares them with normal periods. The study of the relationship between these variables will allow improving the quality of life through new mitigation measures that will minimize the effects of climate change in urban areas. This study analyzes eight cities in the south of Spain (Andalusia) to assess environmental quality through gases SO_2, NO_2, CO, O_3 and aerosols, obtained through Sentinel-5P satellite images, and the LST and SUHI obtained through Sentinel-3 images. Next, the results of periods of heat waves are compared with periods of normal environmental conditions during the summers of the years 2020 and 2021. The objective is to determine the possible impact of heat waves on environmental quality, as well as on the LST and SUHI of the investigated cities, which are located in an area identified as highly vulnerable to the effects of global warming. During the period of the heat wave and compared to the periods without a heat wave, a variety of environmental pollutants was found: SO_2 (+165%), NO_2 (+24%), CO (+8%), O_3 (−4%) and aerosols (+193%). Both the LST and the SUHI suffered an average increase of 2.8 K. The results of this document can help to establish pollutant reduction mechanisms in periods prior to heat waves. This could minimize major effects on the population and provide sustainable development.

Keywords: environmental pollution; surface urban heat island; land surface temperature; heat waves; sentinel 3

Citation: Hidalgo García, D.; Arco Díaz, J.; Martín Martín, A.; Gómez Cobos, E. Spatiotemporal Analysis of Urban Thermal Effects Caused by Heat Waves through Remote Sensing. *Sustainability* **2022**, *14*, 12262. https://doi.org/10.3390/su141912262

Academic Editors: Dimitra Founda and George Katavoutas

Received: 25 August 2022
Accepted: 23 September 2022
Published: 27 September 2022

1. Introduction

Several studies warn that the expansion of urban areas produces an important transformation of the landscape, this being one of the processes that contribute to global warming together with greenhouse gases [1–5]. The construction of new urban areas generates changes in land cover. Namely, there is an increase in the surfaces of waterproof materials for floors and facades (concrete, asphalt, bricks) that reduce evapotranspiration [6]. The absorption of solar radiation increases the net radiation from these surfaces, which is then used to increase sensible heat flux ultimately leading to higher air temperatures [7–9]. Urban areas are the places where there is a greater increase in temperatures compared to rural areas, mainly due to the Urban Heat Island (UHI) phenomenon [3,9–13]. Its intensity presents a high variability due to multiple human activities [14–16] and heat waves. When remote sensing is used to assess the urban heat island phenomenon, we determine the temperature of the Earth's surface and not the ambient temperature. Some investigations indicate that the average air temperature will be 1 to 3 K higher in the coming decades (compared to 1961–1990), by the middle of the century (2040–2069) it will be 3 to 5 K higher and at the end of the century (2070–2100) the increase will amount to 3.5 to 7 K [17,18]. These temperatures are not compatible with the sustainable development of the future [17].

Regarding the state of the art of the investigation, the positive correlation between SUHI and heat waves is somewhat debated: in Maryland and Baltimore [18] 2 K increments are anticipated, Beijing [7,19–21] may see increases between 0.7 and 8 K, New York [22] would undergo an increment of 1 K, Shanghai and Guangzhou [19,20] increments of 1.3 K, Athens [23] 0.2 K increments per decade, Seoul City [24] increases of 3.3 to 4.5 K between the years 2012 and 2016, Dijon (France) [25] increases of 0.7 to 0.9 K from 2014 to 2019, Karachi [26] increases between 0.1 and 3.2 K, Singapore [27] a 2.5 K increment and Madrid would undergo a 1–3 K rise [28].

In sum, numerous studies illustrate the same trend between SUHI and heat waves in urban areas —during periods of heat waves where the temperature intensifies, the same happens to the SUHI. However, the particular climatic conditions, the type of climate and the geographic and morphological factors of the cities also contribute significantly to this interaction [7,20,29–32]. Studies on some European cities [33], Oklahoma [34], London [35], Guangzhou and Beijing [20] report strong increases in SUHI at night. On the other hand, studies in Parma, Athens [36] and Shanghai [20,37] found that the highest increase in SUHI occurs during the morning. Further studies do not show notable amplifications of SUHI [13,22]. Taking into account that the data collection method is similar, the array of results could be interpreted in the sense that coastal cities present a greater intensity during the day while inland cities present a greater intensity at night. This is possibly due to the effect of the sea breeze and differs between cold water (e.g., Chile) and warm water (e.g., Japan) coasts [4]. Recent investigations [38,39] report that gases O_3, aerosols, VOCs (volatile organic compounds) and BVOCs (biogenic volatile organic compounds) are considered a major cause of global warming of the planet. Thus, the study of 361 cities in China during the year 2019 reported that the cities with the highest environmental pollution had higher concentrations of O_3 in the atmosphere, intensifying in the summer period. This was positively related to the variable PM2.5 [40]. In this sense, and with the help of remote sensing, the viability of the Modis aerosol optical depth (AOD) algorithm has been demonstrated for the establishment of environmental pollution control programs [40]. This, in turn, affects climate change through the intensification of extreme weather events, such as heat waves, cold waves, droughts, etc. It is important to carry out new research in these situations of climate change that study jointly the three closely related elements (LST, SUHI and environmental pollution).

Numerous investigations indicate that heat waves occur with increasing frequency, duration and intensity [41,42]. Some studies estimate that by the end of the 21st century they will affect larger regions of the planet [41,43,44]. According to the evolution of these, in the next 40 years, Spain could be one of the countries with large surfaces affected by heat waves in summer. Heat waves are known to have a great environmental, social and economic impact [7]. They imply more water and electricity consumption in homes [45], degradation of air quality [46] and higher morbidity and mortality [2,7,47,48]. Proof can be found in the 1995 Chicago (northern USA) heat wave [48]; in Europe in the summer of 2003 when 70,000 people died [49]; the one that occurred in the summer of 2010 in Russia [50] or that of eastern China in 2013 [51]. In Madrid, between 1979 and 2016, deaths from heat waves increased by 10% [52]. Very recently western Canada witnessed temperatures over 318.2 K for consecutive days that caused about 500 deaths [53].

Although there are numerous methodologies to approach this phenomenon, thermal remote sensing may be most appropriate for large-scale surface temperature studies [5,54]. Studies that rely on Thermal Infrared Sensors (TIRS) have become an important field of research [22]. Among the many investigations include studies of the city of Ganjingzi (China) [54], the Olympic area of Beijing [55], Dwarka river (India) [56], the Chattogram Metropolitan area of Bangladesh [57], the Semarang Metropolitan region [58], Tehran (Iran) [59], Xiamen [60], Wuhan [61] and Changchun (China) [5]. These investigations have allowed researchers to obtain important advances in the studies on UHI. Thus, the laborious task of having environmental data from meteorological stations that are not available or very limited in medium-sized or small cities or located very far from each

other has been eliminated. In this way, it has made it possible to significantly increase the spatial variability of UHI studies up to resolutions of 120 m or 10 m if the high-resolution TsHARP algorithm is used. In turn, it has allowed the study of LST in extensive areas of territory, not limited exclusively to urban areas. Finally, due to the free and open access to the images, it has allowed these studies to be opened up to a greater number of researchers.

Sentinel-3 images are a relatively new high-precision product. The Sentinel-3 features three TIRS bands that allow the LST to be determined at a resolution of 1000 m. It is made up of two satellites: Sentinel 3A and 3B. The fact that it, therefore, orbits every point on the planet twice per day. The use of Sentinel is well documented, for example, in the cities of Huazhaizi and Daman (China) [5], Dahra (Senegal) and Oklahoma City (USA) [62]. The use of the Sentinel-5P space satellite as a monitoring tool for environmental pollutants has been widely used in recent literature. Deserving mention are the environmental studies on eight cities in India [54], four cities in Pakistan [63], 19 cities in India [64] and 11 cities in Europe and the US [65], or the small cities of Passo Fundo (Brazil) [66] and Skopje (Macedonia) [67], shedding valuable light on local concentrations of pollutants.

As indicated above, studies on multiple cities have reported increases in SUHI during periods of heat waves. However, in some cities, these increases are greater during the mornings, in other cities, the intensification has occurred at night and, in others, throughout the day. On the other hand, these studies independently explore the links between heat waves and LST, SUHI and environmental pollution. Recent studies [68,69] establish that the relationship between LST, UHI and environmental pollution occurs due to a transfer process of solar radiation and turbulence processes that are increased by the discharge of pollutants into the atmosphere, highlighting the need to study these elements together. The reduction of vegetation and evapotranspiration, the increase in impermeable surfaces and the increase in anthropogenic heat in urban areas together with environmental pollution increase the effect of UHI. Few studies of the Mediterranean Sea basin explore these variables in conjunction. In light of this, our research aims to provide new evidence connecting heat waves and the three variables indicated. So, it is necessary to carry out new studies that complement the existing ones on the possible synergies and consequences of heat waves on three closely related elements: LST, SUHI and environmental pollution. This relationship may provide the basis for future environmental sustainability and resilience to climate change in cities.

Our research aims to provide a complete analysis of the relationship between heat waves and the three variables indicated. The questions we intended to answer with this study are the following: 1. Can heat waves increase pollutant levels? 2. What influence could heat waves have on the LST and the SUHI? 3. Will this variability be different in daytime and nighttime Sentinel-3 LST values? 4. Can the results obtained in this study influence future urban studies?

2. Materials and Methods

2.1. Study Area and Methodology

2.1.1. Area of Study

The eight cities investigated are located in southern Spain, in the region of Andalusia, which has an area of 87,315 km^2 and a population of 8,329,654. Distinctively, it is the most populated region in Spain and the second largest one (Table 1). According to the Köppen–Geiger climate classification, the region shows different climates. The cities of Cadiz, Granada and Huelva share a Mediterranean Sea climate (Csb), the city of Almeria has a semiarid cold arid climate (Bsh), and the cities of Cordoba, Jaen, Malaga and Seville share a Mediterranean climate (Csa). Hence the region overall has mild, dry summers and humid winters and hot [70]. Andalusia is bordered by the Mediterranean Sea to the south and mountains to the north, which implies that sea and land breezes strongly impact the eight cities studied.

Table 1. Characteristics of cities.

GeographicInformation	Seville	Granada	Cordoba	Jaen	Cadiz	Malaga	Huelva	Almeria
UTM	37.375 N, −6.025 W	37.111 N, −3.362 W	37.891 N, −4.819 W	37.780 N, −3.831 W	36.516 N, −6.317 W	36.765 N, −4.564 W	37.270 N, −6.974 W	36.841 N, −2.492 W
Köppen-Geiger climate	Csa	Csb	Csa	Csa	Csb	Csa	Csb	Bsh
Mean annual T. (K)	291.7	288.7	290.9	290.1	291.5	291.6	290.9	291.1
Average annual rainfall (mm)	576	450	612	552	597	520	467	228
Area (km^2)	141.8	89.8	1263	434	12.3	388	153.3	286.2
Urban (km^2)	69.69	21.88	32.35	9.63	7.44	59.6	14.97	15.95
Population (hab)	687592	234562	324701	111999	115927	573954	143563	198933
Urban mean elevation (masl)	12	681	107	571	14	9	25	17

Climate Zones: Csb: Mediterranean Sea climate; Csa: Mediterranean climate; Bsh: Semiarid cold climate. Source: State Meteorological Agency (AEMET) and National Statistics Institute (NIS).

2.1.2. Method

The method undertaken to develop this research work is outlined in Figure 1. Conversely, the LST of the cities was estimated using Sentinel 3 images, and the environmental pollution values (CO, NO_2, SO_2, O_3 and aerosols) were derived from Sentinel-5P images. Some parts of this methodology have been used in other previous studies obtaining good results [71,72]. The VOCs and BVOCs were not taken into account in this investigation, since they cannot be measured by the Sentinel-5P or by the government meteorological stations. Distinctively, to data from the Andalusian Environment Agency, in accordance with the European Environment Agency (EUROSTAT), the investigated cities present an average annual pollution, according to the Air Quality Index (AQI) criteria, of "good" that increases to "moderate" at certain times of the year where prolonged periods of high pressure and low rainfall prevail. The cities of the study were divided into two typologies, inland, and coastal cities. The plane of LST, SUHI and environmental pollutants was obtained during the different periods investigated, without heat waves and with heat waves. Through these, it was possible to obtain the differences between these variables during these periods. The LST and the environmental contamination obtained through satellite images require a verification process that allows the results obtained to be validated. In the last decades, the comparison method of the LST and the contamination obtained by means of satellite images with the air temperatures and the contamination of the meteorological stations it is of great importance as a verification system for the data obtained by means of the satellite [73–77]. This consists of comparing the LST and contamination recovered with the air temperature and environmental contamination obtained from meteorological stations near the ground (1.5 m). Through this system, the statistical variables take on importance including the R^2 regression coefficient, the mean error bias (MBE) and the root mean square error (RMSE). In our research, and in order to verify the LST and pollution values obtained through Sentinel 3 and 5P satellite images, they have been compared with the air temperature and environmental pollution values obtained by the meteorological stations owned by the State Agency for Meteorology (AEMET) during the hours of passage of the satellites. Each city has a weather station whose data can be consulted free of charge. The Data Panel statistical method allows one to include in the overall result any individual effects that each city may have owing to its particularities. This method has been corroborated by similar studies [78–80] involving time series of multiple sites when, in addition, the conditions of the different cities analyzed may vary.

2.2. Data Source

2.2.1. Heat Waves

In 2020, according to Spain's State Meteorological Agency (AEMET), two episodes were classified as heat waves in Andalusia; in 2021, two episodes were also classified. The AEMET defines a heat wave as an episode of at least three consecutive days during which a

minimum of 10% of the state stations considered register maximum ambient temperatures above the 95% percentile of their series of maximum daily temperatures for the months of July and August in the period 1971–2000. Table 2 offers the data and characteristics of the heat waves (start date, end date, duration, maximum temperature and thermal anomalies) studied here.

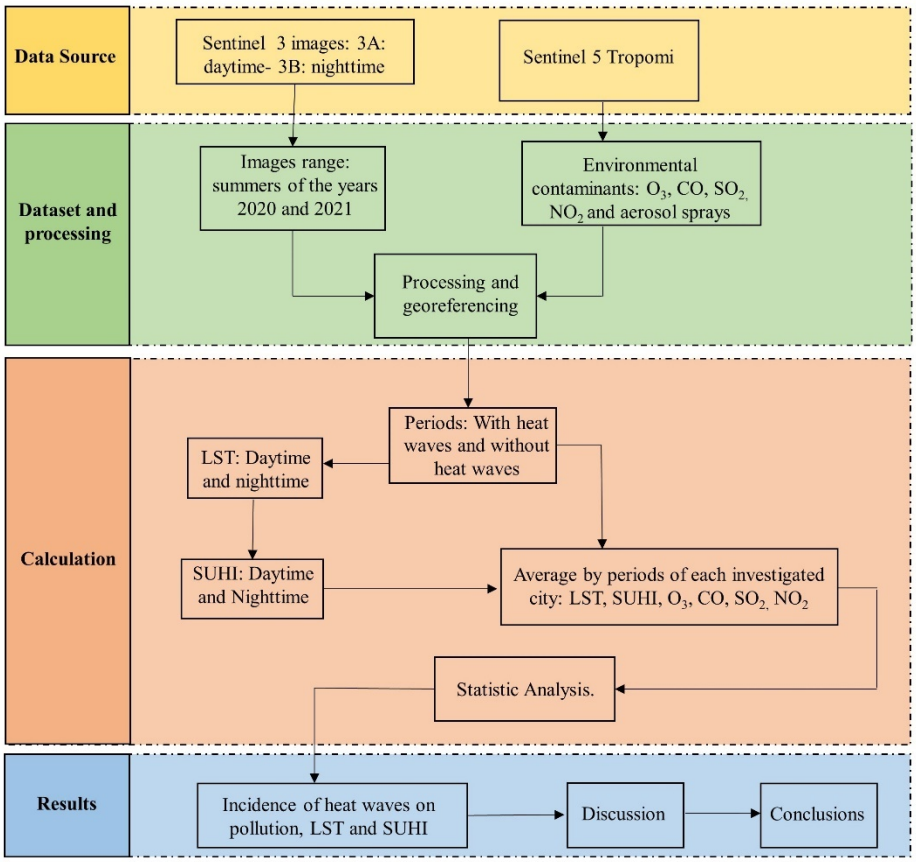

Figure 1. Description of the methodology.

Table 2. Characteristics of heat waves.

Heat Waves	1st (2020)	2nd (2020)	3rd (2021)	4th (2021)
Start date	25 July 2020	5 August 2020	11 August 2021	21 July 2021
End date	2 August 2020	10 August 2020	16 August 2021	23 July 2021
Duration (days)	9	6	6	3
Air thermal anomaly (K)	3.1	2.5	4	1.9
Maximum air temperature reached (K)	310.15	312.15	312.65	310.7

Source: State Meteorological Agency (AEMET).

The four heat waves investigated were detected at all AEMET weather stations in Andalusia (Spain). We compared the LST and the SUHI under conditions without heat waves and heat wave conditions. For the period without heat waves, the six days before and after the heat waves were taken into account, giving a characterization of normal periods based on 27 days that are close in time to heat waves.

2.2.2. Sentinel 3—Images

Sentinel-3 satellites have a temperature measurement instrument—the Sea and Land Surface Temperature Radiometer (SLSTR)—with 21 bands, a spatial resolution ranging between 300 and 1000 m and a wavelength from 550 µm to 12,000 µm. Sentinel products feature three levels of processing (0, 1 and 2), although only the latter two are available for

scientific use. Those of level 1 present brightness temperatures that require determination of the ground emissivity to derive the LST. As part of the level 2 set of SLSTR operational products, the LST is derived using a split-window formulation.

The area under study lies below the path of both Sentinel 3A and 3B, which respectively pass overhead at around 10:00 am or 09:00 pm. The images selected for our research, corresponding to twenty-five days in July and August 2020 and 2021, present a cloudiness index of less than 10%. Therefore, the time series of the data used was 51 days distributed between the months and years indicated. Of these, 24 days correspond to heat wave conditions and 27 days correspond to non-heat wave conditions. It must be taken into account that day and night images of LST were obtained for each day. This ensures greater visibility and precision in the LST and subsequent calculation of the SUHI. The urban LST and pollution values used in this research correspond to the mean values of the pixels included within the contour that delimits the urban area after a reclassification process at 100 m. The pre-processed level 2 images used were downloaded from the Copernicus Open Access Hub of the European Space Agency (ESA) (https://scihub.copernicus.eu/ (accessed on 10 January 2022)); they give the emissivity of the ground and the water vapor content of the atmospheres recorded by the satellite itself. Copernicus open software environment was used: Sentinel Application Platform (SNAP), version 8.0.0. All images were reclassified and corrected. After this procedure, the LST images, by means of the open-source software QGIS 3.22.10, were exported to Geotiff format.

2.2.3. Environmental Variables CO_2, SO_2, O_3, NO_2 and Aerosols

The values of the environmental pollution variables O_3, SO_2, NO_2, CO and aerosols were collected using the tropospheric monitoring instrument (TROPOMI) integrated into the Sentinel-5P satellite. A total of 51 Sentinel 5P images coinciding with the days of the Sentinel 3 images were used so that the information established between LST, SUHI and contamination coincided in the days. Therefore, a total of 51 days of Sentinel 5P images were used, 24 days without a heat wave and 27 days with a heat wave. Some studies [54,64] have used and calibrated the values of Sentinel 5P, obtaining a high concordance of the contamination data. Sentinel 5P has 7 bands with a minimum spatial resolution of 3500 m and scans the Earth's surface daily using four high-resolution spectrometers. The time of passage of the Sentinel-5P satellite over the cities of study is between 12:00 noon and 1:00 pm. A total of 150 images were acquired through ESA's Copernicus Open Access Hub for level 2.

2.2.4. Land Surface Temperature Estimation (LST)

The algorithm that Sentinel uses internally in the products to assess the LST is based on the concept of absorption difference [81]. The molecules of the atmosphere absorb the wave radiation that is captured by the Sentinel bands to which an atmospheric correction is subsequently applied. Previous studies attest to the accuracy of these algorithms in Sentinel-3 images [82]. The SLSTR Sentinel product algorithm internally includes the ground emissivity according to Equation (1) [83,84]:

$$LST = a_0 + b_0 \left(T_{11} - T_{12}\right)^{\frac{1}{\cos\left(\frac{\theta}{m}\right)}} + \left(b_0 + c_0\right) T_{12} \quad (1)$$

where LST is the temperature of the Earth's surface in K; a_0, b_0 and c_0 are coefficients that depend on land cover type, vegetation fraction (biome), season, time of day (day or night) and is the atmospheric column water vapor content (in cm). T_{11} and T_{12} are the brightness temperatures (top-of-the atmosphere) in the upper part of the atmosphere on bands 11 and 12, respectively. In turn, θ is the zenith angle of view of the satellite located in the metadata file, while m is a variable parameter controlling the dependence on view angle [84,85].

2.2.5. SUHI Estimation

SUHI is described in the literature as the temperature difference between an urban area and a rural area taken at the same time [86]. The delimitation between urban and rural areas was carried out manually using the QGIS software with the help of high-resolution Sentinel 2 satellite images. The built-up areas were included within the urban areas and the rest were in rural areas. It can be determined according to Equation (2).

$$\text{SUHI} = \text{LST}_{\text{urban}} - \text{LST}_{\text{rural}} \quad (2)$$

The urban LST values correspond to the mean values of the pixels located within the urban area of the investigated cities. The pixels located between the urban and rural areas were cut taking into account only the part that is within the urban area. The rural areas chosen to derive the SUHI through the temperature difference with urban areas given correspond to the places where AEMET has rural meteorological stations, some 10–30 km away from urban centers. After exporting the LST images obtained from Sentinel 3 to the QGIS software, the SUHI of the cities could be determined with the help of Equation (2). The considerations behind choosing an AEMET rural station were [87]: (1) The percentage of impermeable soils in the station should not be higher than 20%, and the proportion of agricultural land should be higher than 70%; (2) A difference in altitude between the city and the rural station of only approximately 50 m; (3) Rural stations had to be outside urban areas; and (4) The station must be located in an area of approximately equal surface coverage of 1000×1000 m^2.

2.2.6. Strategy of Analysis

Panel data refers to a type of statistical analysis that combines a temporal dimension (time) with a cross-sectional dimension (data or values). This method is often cited in the literature nowadays, and it involves the use of multiple regression models [78–80], so that a larger amount of data may be included than under traditional methods. It is compatible with three calculation options: ordinary squares method (OSM), generalized least squares (GLS) and intragroup estimation method (IEM) [88]. To know which of them is best, the following steps must be carried out [79]: (1) Using the Hausman test, determine if the effects of the analysis are fixed or random. This allows the method to determine different hypotheses about the behavior of the residuals of statistical analysis. (2) Evaluation of the model using the Wooldridge and Wald tests. Both phases will indicate the most appropriate method to use [89]. In our case, statistical analysis was performed with STATA software, version 16; and after carrying out the indicated tests, the IEM method with random effects was used according to Equation (3):

$$Y_{it} = \beta\, X_{it} + \alpha_i + \mu_{it} \quad (3)$$

where μ_{it} is the error of the model, α_i represents the individual effects, X_{it} are explanatory variables, β is an independent variable.

This method allows for a greater amount of data in the analysis, thereby increasing the degree of freedom, while reducing inconvenient collinearity between the variables. By taking into account individual (each variable analyzed) effects, the final function obtained for the set of individuals (each city analyzed) is totally different from the one that would have been obtained using other statistical techniques. It is assumed that individual effects are not reflected in the explanatory variables of the model; instead, they contribute to the error term. Therefore, the equation determines the results globally for all the cities, but the data is entered individually by city. Obtaining data from satellite images for statistical analysis was performed by randomly determining a certain number of points per image. For the 4 heat waves analyzed between 2020 and 2021, a total of 400,000 data were collected on the LST, SUHI and environmental pollutant variables.

3. Results

3.1. LST Validation and Contamination

The validation results of the LST and environmental contamination values obtained from Sentinel 3 and 5P can be seen in Table 3.

Table 3. Sentinel 3 and 5P validation data.

Heat Waves	R^2	RMSE	MBE
LST	0.93	2.34 K	−0.12 K
O_3	0.92	0.02 μm/m^3	0.01 μm/m^3
CO	0.91	0.01 μm/m^3	0.02 μm/m^3
SO_2	0.94	0.0001 μm/m^3	0.0004 μm/m^3
NO_2	0.91	2×10^{-6} μm/m^3	2×10^{-7} μm/m^3
Aerosol	0.95	0.02 μm/m^3	−0.003 μm/m^3

3.2. Land Surface Temperature (LST)

Figures 2 and 3 show the mean differences in daytime and nighttime LST between the periods without and with the heat wave. Figures S1 and S2 in Supplementary Materials show the mean values of daytime and nighttime LSTs without and with a heat wave.

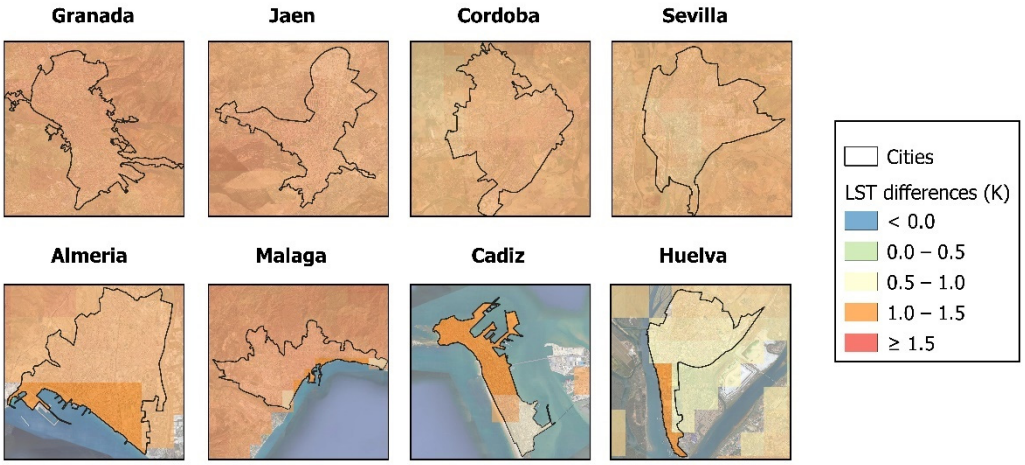

Figure 2. Daytime LST differences between periods with and without heat wave.

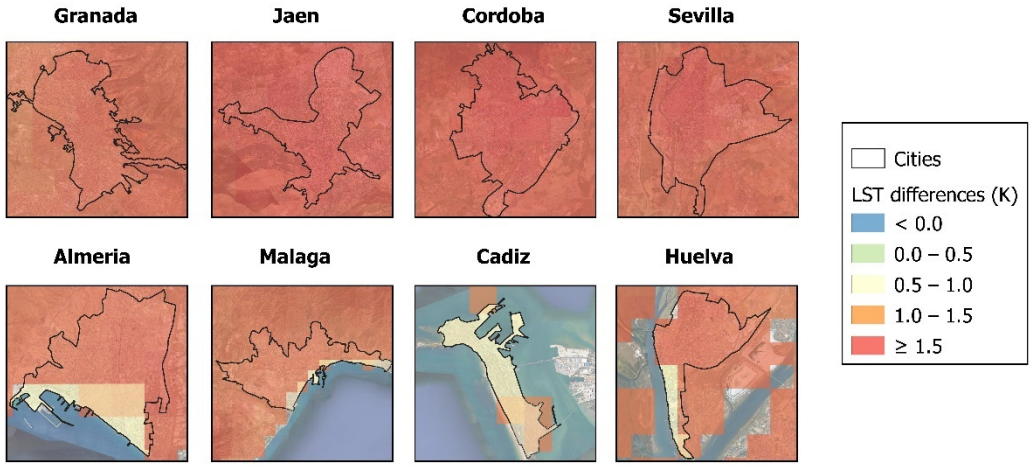

Figure 3. Nighttime LST differences between periods with and without heat wave.

Figure 4 displays the LST values obtained from Sentinel daytime and nighttime images for the periods without a heat wave and with a heat wave. In all eight cities investigated, during the heat wave periods, diurnal LST values were higher than those obtained under

conditions without heat waves. The average rise in LST for the eight cities was found to be 3.6 K, the highest increases occurring in the coastal cities of Huelva (8 K) and Malaga (6.1 K). The smallest increases were seen in the cities of Cordoba and Cadiz (1.6 K). The night LST values during the heat wave period were significantly higher than the values recorded at times without heat waves. The average increase in LST in the eight cities was 2 K, the largest increases occurring in Huelva (3.6 K) and Seville (3.5 K). In contrast, the coastal cities of Almería (0.6 K) and Cadiz (0.8 K) gave the smallest increases.

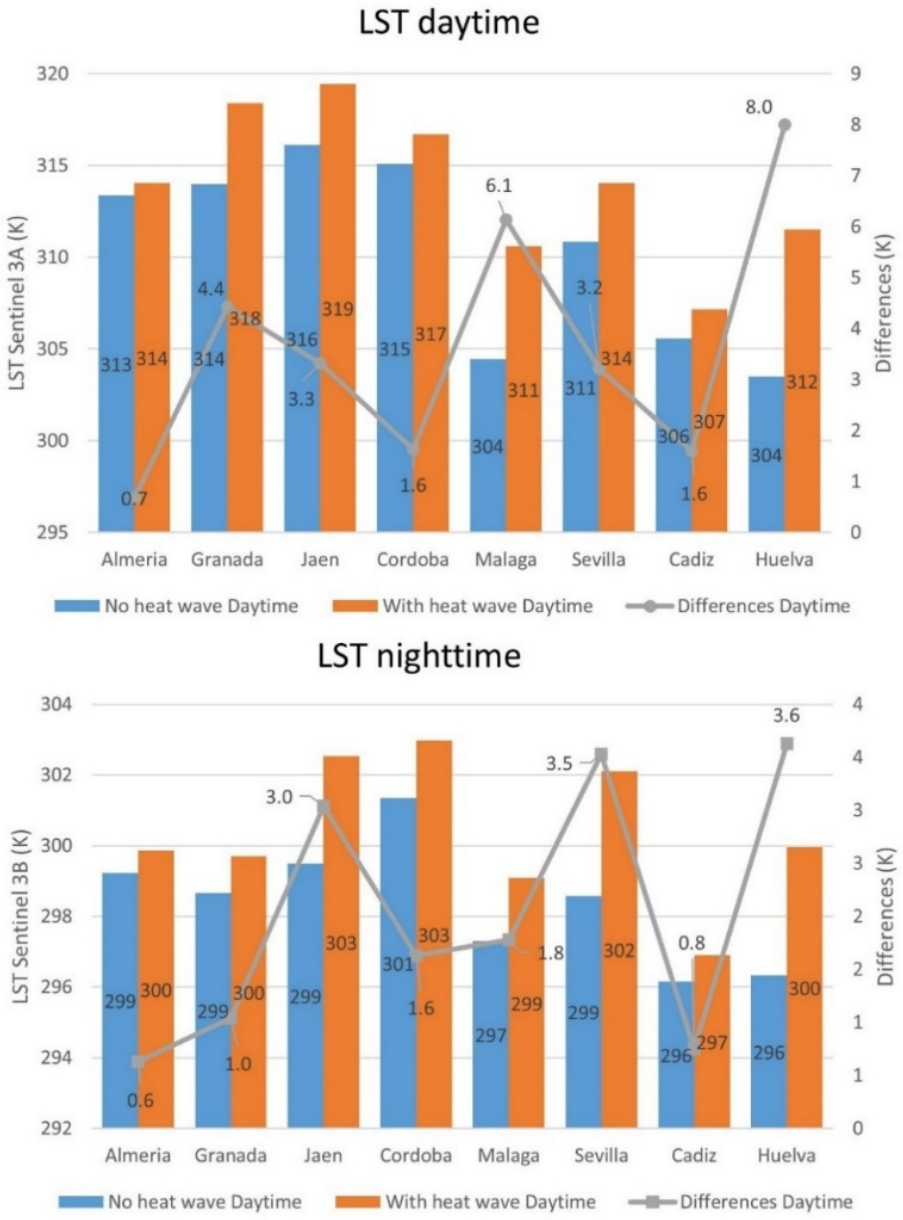

Figure 4. Average day and night LST by city.

Figure 5 illustrates how the increases in LST generated by heat wave situations present strong spatial and temporal variability. Our results show that the increase in daytime LST was greater in cities located on the coast (an increase of 4.1 K) than in inland cities (a rise of 3.1 K), possibly due to the effects of the breeze. In turn, according to Sentinel 3B data, the increase in LST was greater in inland cities (2.7 K) than in coastal cities (1.7 K). Based on the results obtained, it can be stated that both the day and night LSTs underwent significant increases during the heat wave period; but the mean increase is greater for the daytime reading (3.6 K) than at night (2 K).

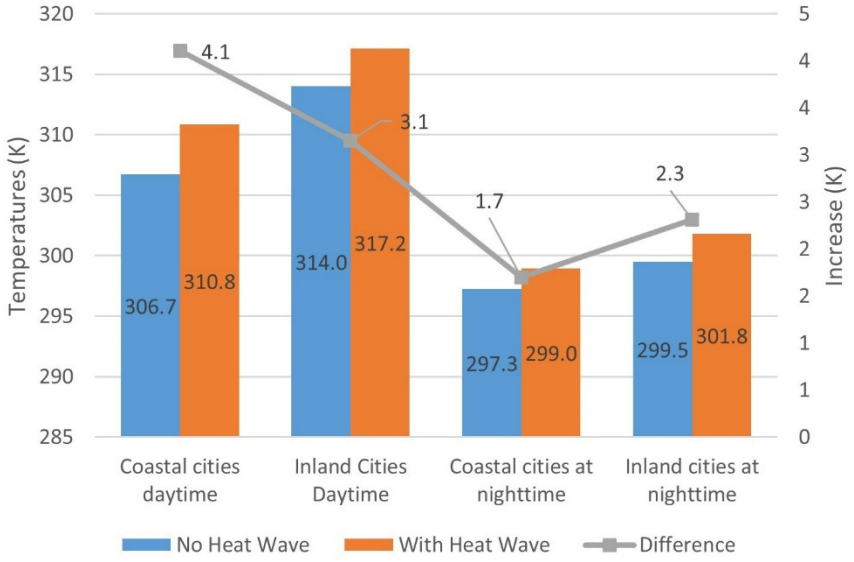

Figure 5. Average increases in LST according to city group.

3.3. SUHI

The SUHI results indicate average increases of this phenomenon during periods of heat waves, from 0.5 K to 5.3 K, with a mean value of 2.8 K. Figure 6 offers the daytime SUHI values both for conditions without heat waves and for the periods of a heat wave.

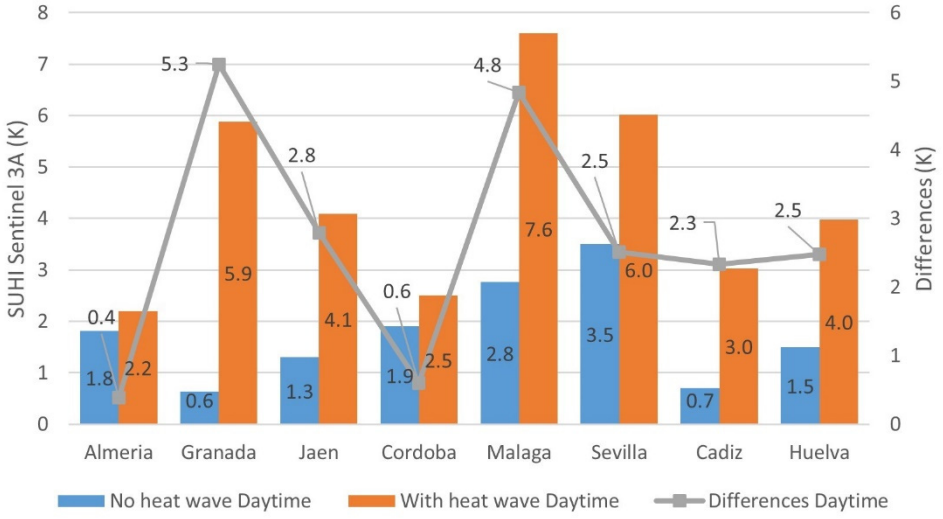

Figure 6. Daytime SUHI averages by city.

The average diurnal intensity of the SUHI under conditions without heat waves was 1.8 K, while during the heat waves it increased to an average of 4.4 K. The greatest SUHI increases were seen for Granada (5.3 K) and Malaga (4.8 K); the smallest increases were seen for Almeria (0.4 K) and Cordoba (0.6 K). In Figure 7 and according to the Sentinel 3B images, the nocturnal SUHI values for different periods are shown.

The average nighttime intensity of the SUHI under conditions without heat waves was 1 K, while during the heat wave period it increased to a mean value of 3.8 K, an average increase of 2.8 K. The largest increases in the intensity of SUHI were seen in the cities of Cadiz (6 K) and Granada (4.5 K), contrasting with the lowest values, those of Malaga (0.7 K) and Cordoba (1.3 K). As illustrated in Figure 8, the SUHI increases in the cities of Andalusia generated by the environmental circumstances of heat waves present strong temporal and geographic variability.

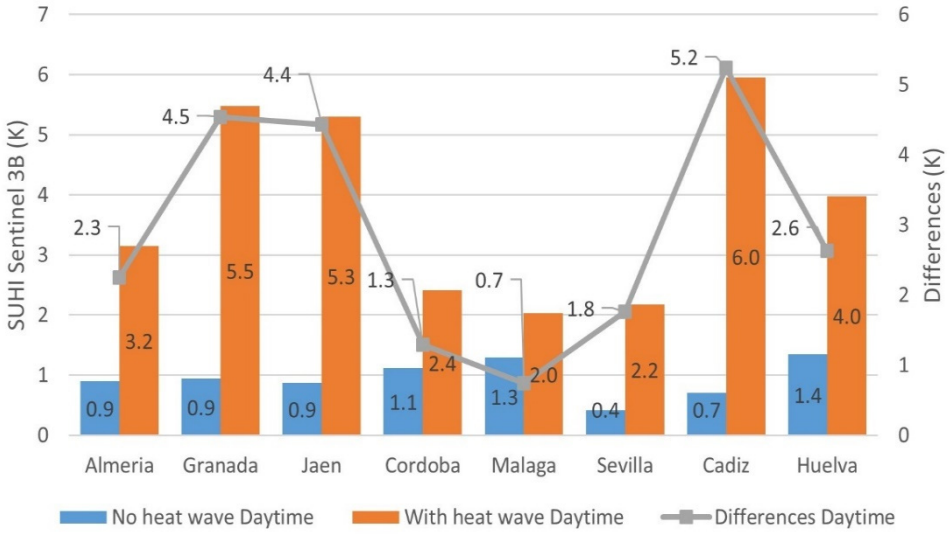

Figure 7. Nighttime SUHI averages by city.

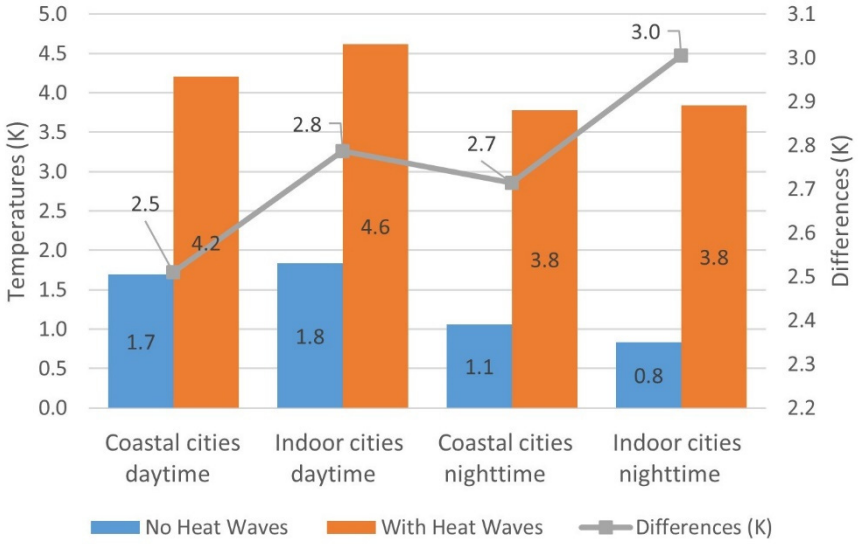

Figure 8. Average increases in SUHI according to type of city.

The increase in SUHI is greater in inland cities (2.8 K) than in coastal cities (2.5 K). The data by Sentinel-3B likewise indicate a greater increase in nighttime SUHI for inland cities (3 K) than for coastal ones (2.7 K). It can therefore be affirmed that the heat wave situation causes an increase in the daytime and nighttime SUHI intensities. Indeed, the increase in SUHI presents similar mean values during the day (2.7 K) and at night (2.9 K).

3.4. Environmental Contaminants

The average pollution concentrations that were taken into account for the study cities (SO_2, NO_2, CO and aerosols) suffered significant increases during the heat wave periods compared to the average values for the periods without a heat wave. However, O_3 values showed decreases during the same periods. Figures 9–13 show the differences in contaminants found between the different periods. Figures S3–S7 in Supplementary Materials show the average concentrations of pollutants during the periods of heat waves and periods without heat waves. Thus, the figures for the heat wave periods include the mean values of the three waves studied, while the others express the mean values for the days/periods of conditions without heat waves.

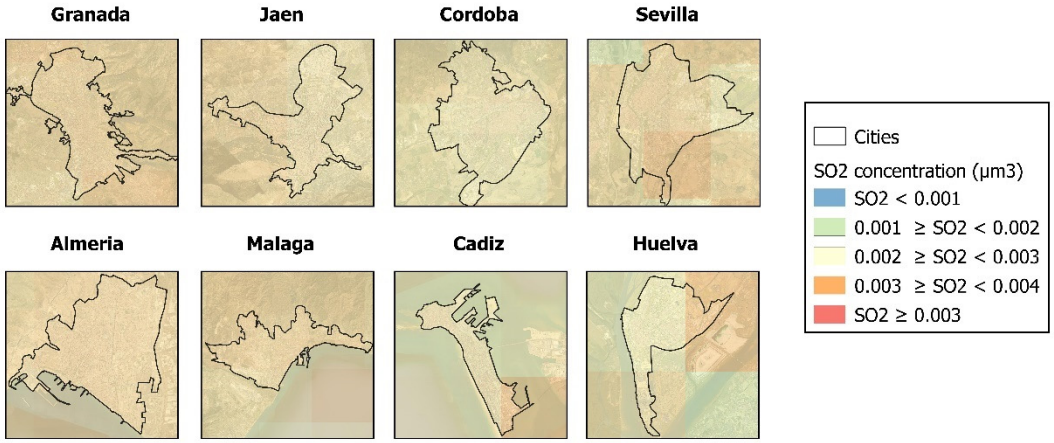

Figure 9. SO_2 Sentinel 5P differences between periods with and without heat wave.

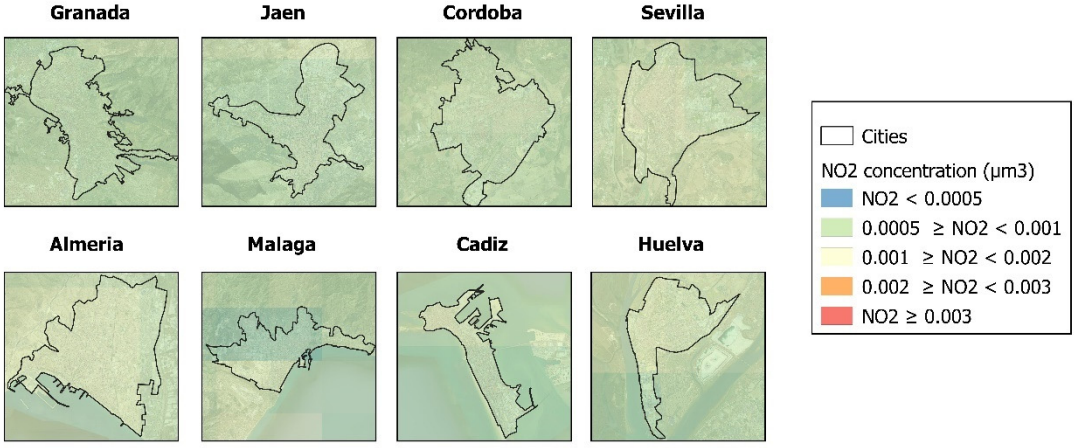

Figure 10. NO_2 Sentinel 5P differences between periods with and without heat wave.

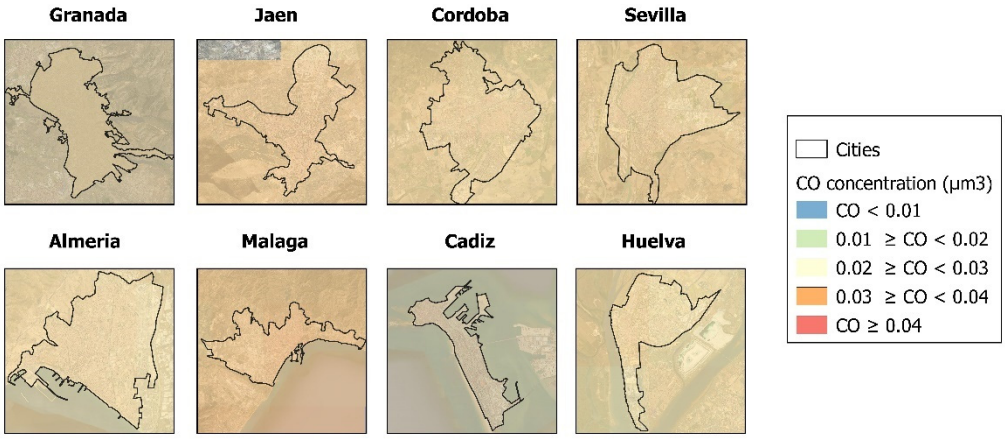

Figure 11. CO Sentinel 5P differences between periods with and without heat wave.

Figure 14 shows, for all the cities, the mean values of the variables investigated both in periods without heat waves and in periods with heat waves. The increases in pollutant concentrations during periods with heat waves for all the cities studied were aerosols (193%), SO_2 (165%), NO_2 (24%) and CO (8%). A decrease in the O_3 variable of 4% was also registered.

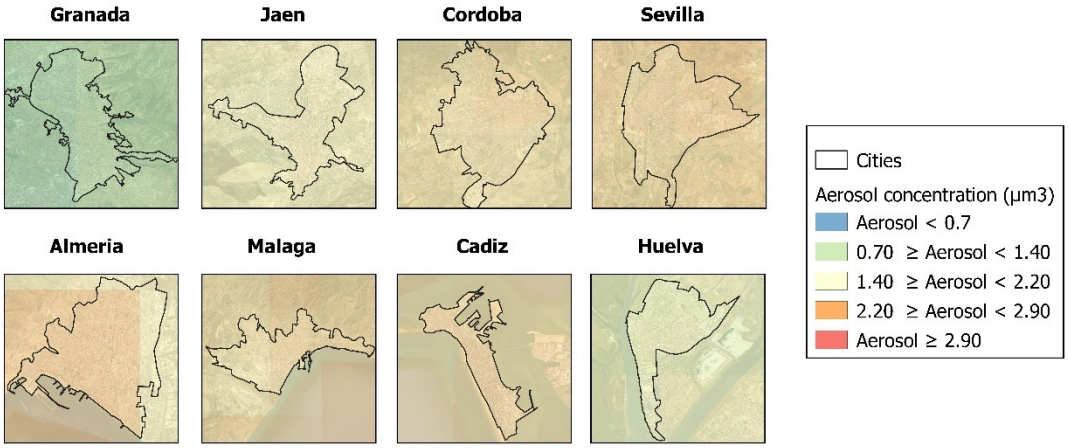

Figure 12. Aerosol Sentinel 5P differences between periods with and without heat wave.

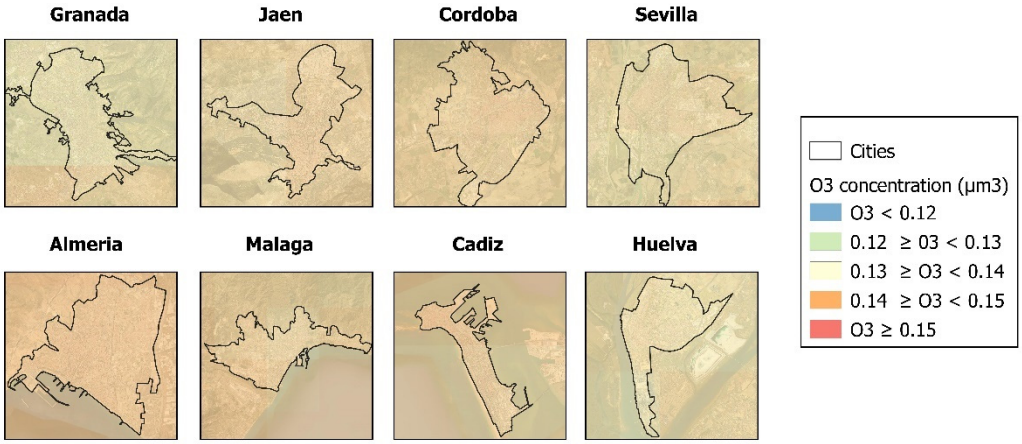

Figure 13. O_3 Sentinel 5P differences between periods with and without heat waves.

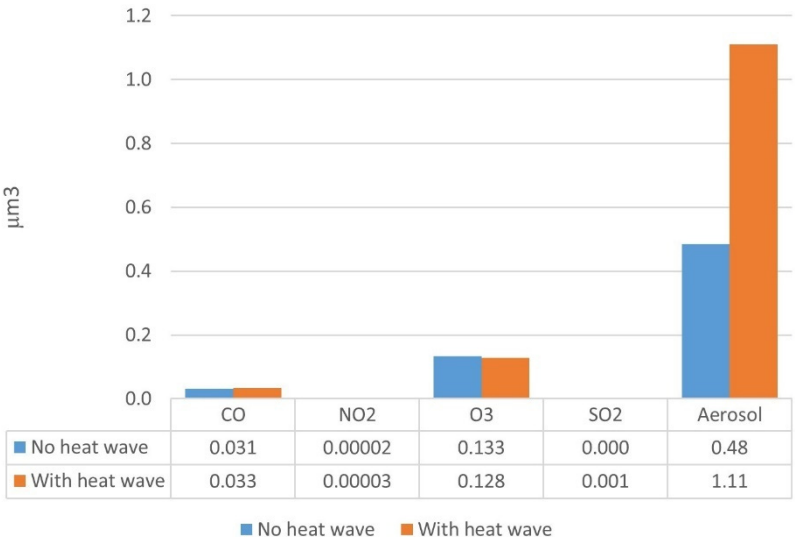

Figure 14. Variability of the average concentration of global pollutants, taking into account all the cities.

Figure 15 shows the variations suffered by the pollutants by period analyzed and city typology: inland vs. coastal. The average values of the two periods analyzed (with and without heat waves) are given. Clearly, the SO_2 pollutants and aerosols present high spatial variability with regard to the type of city. Pollutants CO, NO_2 and O_3 present

similar values, increasing in both types of cities during heat wave periods. Inland, the average increases are: SO_2 (+205.6%), aerosols (+87.4%), NO_2 (+21%) and CO (+8.2%), while the decrease in variable O_3 is −2.8%. The average increases in coastal cities are aerosols (+197.2%), SO_2 (+78.9%), NO_2 (+25.6%) and CO (+7.6%); the decrease in O_3 is −5.6%. It is necessary to indicate that the SO_2 measurements of the coastal cities could be affected by the maritime circulation of the ports. However, taking into account that since the circulation is continuous, it would affect both the values obtained during the periods without a heat wave and during the periods with a heat wave analyzed, it would not alter the differences obtained between both periods.

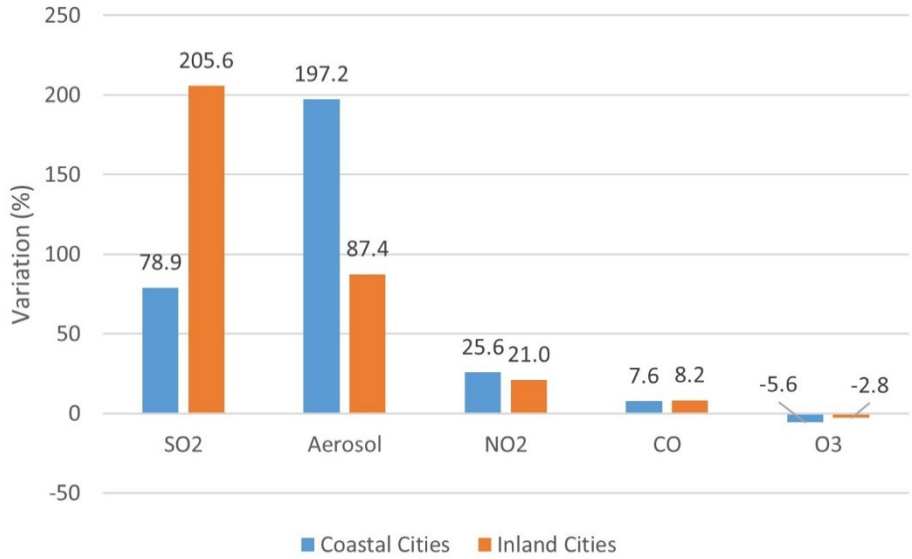

Figure 15. Variation (%) of pollutants by city type and period analyzed.

In sum, the largest increase in environmental aerosols during heat wave periods was found to occur in coastal cities, while the largest increase in SO_2 is seen in inland cities. The pollutant that shows the greatest reductions is O_3, which undergoes a greater drop in coastal cities. Accordingly, the heat wave climatic situation produced a generalized increase in environmental pollutants, whereas O_3 decreased in both city types studied.

3.5. Statistical Analysis of Data

For the statistical analysis of Sections 3.5.1 and 3.5.2 the dependent variables have been the LST and SUHI while the independent variable has been the environmental conditions of heat waves. On the contrary, and for the analysis of Sections 3.5.3 and 3.5.4, the dependent variable has been the heat wave conditions while the independent variables have been the environmental pollutants.

3.5.1. LST and SUHI Versus Heat Waves Situation

The Panel Data analysis technique was used to determine if heat waves alter the SUHI and the LST. As indicated in Section 2.2.6, the method followed is the GLS with random effects according to the Hausman test and according to Equation (3). Results can be seen in Tables 4 and 5. The beta value indicates the number of units that the LST and the SUHI (K) increase for each higher unit of the independent variable (heat wave). The greatest increases in the LST occur during daytime readings; the greatest rises in SUHI occur at nighttime. The LST values convey a statistically positive and significant 95% relationship between the heat wave situation and the LST. Furthermore, the Sentinel daytime results yield a statistically significant and positive relationship of 99% between the SUHI variables and the atmospheric heat wave situation. This relationship is greater than 99% with the values obtained using nighttime data.

Table 4. Panel data statistical analysis of heat waves influence on LST.

	Daytime			**Nighttime**		
	β	*p*	sd	β	*p*	sd
LST	3.627	*0.042* *	2.329	0.120	*0.049* *	0.057

β: Regression coefficient; *p* value: * $p < 0.05$; sd: standard deviation.

Table 5. Panel data statistical analysis of heat waves influence on SUHI.

	Daytime			**Nighttime**		
	β	*p*	sd	β	*p*	sd
SUHI	0.175	*0.004* **	0.050	0.223	*0.000* ***	0.044

β: Regression coefficient; *p* value: ** $p < 0.01$ and *** $p < 0.001$; sd: standard deviation.

The F statistic of an analysis assesses the explanatory power of the independent variable over the dependent variable, while R^2 and Prob > chi^2 determine whether there is a significant difference between the expected and observed results. These values are given in Table 6. The first is used to assess the explanatory power of the independent variable with respect to the dependent variable. The second indicates the importance of the relationship between the variables. It can therefore be said that there is a statistically significant relationship between the LST and the SUHI in both periods investigated. Still, this relationship is stronger during periods of heat waves with the SUHI than with the LST. These statistical data are consistent with the data expounded in the previous section. The data distribution assumptions were tested using the Kernel density method. This method and through the study of the histogram allow us to determine if the data present parametric behaviors or not. Kernel results for our data presented a homogeneous distribution.

Table 6. R^2 and F statistical analysis of heat waves situation.

	Daytime			**Nighttime**		
	R^2	F	Prob > chi^2	R^2	F	Prob > chi^2
LST	0.383	2.434	0.002	0.451	4.484	0.003
SUHI	0.463	12.146	0.004	0.649	24.771	0.000

R^2: Linear regression coefficient; F: F statistic.

3.5.2. Variability of the SUHI and LST with the Type of the City Investigated

Next, we calculate the relationship between the SUHI and LST according to the type of city. For this, and through Equation (3), the GLS method was applied. Table 7 shows the results obtained. It is observed that the largest increases in LST and SUHI occur during daytime readings in inland cities, whereas the largest increases in SUHI occur in nighttime readings and in coastal cities. Statistical analysis of daytime data reflects a positive relationship between heat waves and LST in coastal cities, at 95%. Contrariwise, for nighttime data, inland cities show a positive and significant relationship at 95%. With respect to the SUHI, daytime data indicate that in the morning there is a 95% positive relationship between heat waves and SUHI only in inland cities. According to the nocturnal data, the statistically positive relationship at 95% occurs in both types of cities. We may thus affirm that the statistically significant relationship is stronger in inland cities in both daytime and nighttime readings when compared to coastal cities. These statistical data are consistent with the data put forth in the previous section.

The results of statistical analysis, reflected in Tables 7 and 8, indicate that the daytime LST presents a more intense relationship with heat wave occurrence in coastal cities, whereas the nighttime LST relationship is stronger for inland cities. In the case of SUHI, the daytime and nighttime relationships occur with greater intensity in inland cities. These statistical relationships are consistent with the results described in the analytical calculation section. However, during periods of heat waves, this relationship is stronger with the SUHI

than with the LST, in view of the F statistic. Again, these findings would be consistent with the data given in the previous section.

Table 7. LST and SUHI Sentinel 3A and 3B results by city type.

	Daytime						**Nighttime**					
	Inland Cities			**Coastal Cities**			**Inland Cities**			**Coastal Cities**		
	β	*p*	sd	β	*p*	Sd	β	*p*	sd	β	*p*	sd
LST	0.121	0.103	0.629	0.069	0.015 *	0.045	0.210	0.045 *	0.088	0.191	0.141	0.113
SUHI	0.197	0.036 *	0.073	0.158	0.094	0.080	0.215	0.016 *	0.065	0.234	0.018 *	0.072

β: Regression coefficient; *p*: *p* value: * $p < 0.05$; sd: standard deviation.

Table 8. Statistical analysis: R^2 and F, Sentinel 3A and 3B, by type of city.

	Daytime						**Nighttime**					
	Inland Cities			**Coastal Cities**			**Inland Cities**			**Coastal Cities**		
	R^2	F	Prob > chi^2	R^2	F	Prob > chi^2	R^2	F	Prob > chi^2	R^2	F	Prob > chi^2
LST	0.38	3.68	0.1034	0.28	2.37	0.1749	0.48	5.65	0.0551	0.33	2.87	0.141
SUHI	0.54	7.28	0.0357	0.39	3.95	0.0941	0.64	10.96	0.0162	0.63	10.41	0.018

R^2: Linear regression coefficient; F: F statistic.

3.5.3. Environmental Pollutants during Heat Waves

In a new phase of statistical analysis, we sought to determine whether the heat wave affected the concentration of pollutants. For this purpose, and following the method described above, Panel Data was performed in conjunction with the GLS method and random effects through equation 3. The results are expressed in Table 9. According to the table, a negative relationship of 95% is seen with the variable O_3 and a positive relationship with the variables SO_2 and aerosols. These statistical data support the data given above. The environmental pollutants data show a regular distribution according to the Kernel test.

Table 9. Environmental pollutants under heat waves.

Variables	**Sentinel 5P**		
	β	*p*	sd
CO	60.4375	0.233	47.5893
NO_2	10,664.9	0.421	12,699.14
O_3	−42.922	0.013 *	14.2939
SO_2	182.793	0.038 *	76.3555
Aerosol	0.4559	0.037 *	0.19013

β: Regression coefficient; *p*: *p* value: * $p < 0.05$; sd: standard deviation.

3.5.4. Variability of Pollutants by Type of City Investigated

Our statistical analysis aimed to determine the variability of environmental pollution according to the type of city: inland or coastal. After determining that it was necessary to use the Panel Data with random effects, the GLS method was applied through equation 3. The results for each city type are expressed in Table 10. In inland cities, a 95% positive relationship is detected between the variable SO_2 and the heat wave. For coastal cities, a 95% relationship is likewise reported between SO_2 and aerosols with heat waves, and a 95% negative relationship with the variable O_3.

The values of R^2, F statistic and Prob > chi^2 obtained are represented in Table 11. There is a good concordance between the variables investigated by the method used, with an adjustment level raised to 95% of significance. The values reflected in Tables 10 and 11 indicate that pollutants present a more intense relationship in coastal cities than in inland

cities, as the former have a higher F statistic. These statistical relationships are consistent with the results obtained by means of analytical calculations.

Table 10. Statistical analysis of environmental variables by type of city.

Variables	Inland Cities			Coastal Cities		
	β	*p*	sd	β	*p*	sd
CO	113.92	0.310	84.44	10.066	0.830	41.259
NO_2	12,824	0.494	15,466	−4874	0.771	14,541
O_3	−28.32	0.191	14.566	−84.08	0.029 *	14.690
SO_2	232.75	0.043 *	61.53	111.85	0.035 *	115.36
Aerosol	0.5940	0.255	0.376	0.4156	0.022 *	0.1266

β: Regression coefficient; *p*: *p* value: * $p < 0.05$; sd: standard deviation.

Table 11. R^2 and F Sentinel 5P statistical analysis by city type.

	Inland Cities			Coastal Cities		
	R^2	F	Prob > chi^2	R^2	F	Prob > chi^2
Variables	0.97	13.10	0.072	0.98	20.10	0.048

R^2: Linear regression coefficient; F: F statistic.

4. Discussion

Overall, the results reported here point to significant increases in the LST, SUHI and environmental pollutants analyzed during periods of heat waves in comparison to periods without heat waves. The LST and SUHI increased by 2.8 K; aerosols, SO_2, NO_2 and CO showed average increases of 193%, 165%, 24% and 8%, respectively. These findings were corroborated by statistical analysis. Heat waves are associated with high pressures that decrease wind speed and cloud cover. This causes more solar radiation to be received, which leads to an increase in temperatures. Such circumstances amplify the SUHI phenomenon and the concentration of environmental pollutants [86,90,91]. The strong warm anticyclonic conditions coming from North Africa are often associated with heat waves in Spain [92–94]. Investigations involving other cities/territories report results similar to ours for periods of heat wave [18,22,95–98]. For instance, in the Netherlands, a heat wave in the summer of 2003 produced an increase in PM_{10} concentrations and excess mortality [95]. In the city of Moscow, the summer heat wave of 2010 likewise increased ambient temperatures and concentrations of PM_{10} and CO [98]. Our findings confirm that a heat wave situation can bear an impact on the environment in terms of more pollutants. The fact that O_3 showed an average daily decrease of 4% during the heat wave period is also in line with previous reports [21,99–101]. This situation is motivated by various circumstances that occur in the area under study. On the one hand, O_3 in the presence of NO reacts to form NO_2. Therefore, the concentration of O_3 is usually low in urban centers and higher in rural areas. The radiative effect of aerosols is another element of great importance. Higher concentrations of aerosols attenuate O_3 production. Our results have reported increases in NO_2 and aerosols, so a reduction in O_3 is evident. Winds from the south have lower speeds and generate higher O_3 concentrations [101]. In the cities studied, the winds in situations without a heat wave come from the south but in situations of a heat wave, they come from the north. This circumstance justifies this situation of O_3 reduction.

Temporal variability in pollutant increases is more evident in inland cities than in coastal areas. The total mean value, for all study days, is higher in the first (80.50%) than in the second (77.30%). The pollutant that increases the most in inland cities is SO_2, while aerosols experience the greatest increase in coastal cities during a heat wave situation. Statistical analysis pointed to stronger relationships between pollutants and coastal cities during periods of heat waves. This is due to the fact that SO_2 is generated by power plants that operate at higher performance levels in periods of heat waves to guarantee the electricity supply of air conditioning systems. In Andalusia, the generation plants are

located in the inland regions, very close to the cities. Therefore, it would be logical to assume that in periods of heat wave, SO_2 is higher in inland cities. This situation has been corroborated by other investigations in metropolitan Kolkata (India) [102] or in the Indo Gangetic Basin (North India) [103].

The largest increase in aerosols observed in coastal cities can be attributed to a major source known as maritime aerosols, which are carried by the wind along coastal areas. This situation has already been studied previously in other similar investigations, reaching the same results obtained here [63,103]. This circumstance allows pollutants CO, NO_2 and O_3 to present similar values, increasing in both types of cities during heat waves. This is due to the fact that in Spain, heat waves are related to strong anticyclonic conditions due to the great height of the ridge, which ensures clear skies and significant solar irradiation, together with high warm advection coming from North Africa. This produces a stagnation of atmospheric pressure and a decrease in wind speed, which implies a higher concentration of pollutants. Similar situations have been reported in other cities or areas of the planet, such as Singapore [104] or in India [105], allowing the results presented here to be validated. The values reported here support previous findings for coastal or inland territories that suffered periods of heat waves [2,33,54,56,95,97,102,103,106].

Our results indicate significant increases in LST during periods of heat waves, with an average value of 2.8 K. Specifically, the average daytime LST of the investigated cities shows an average increase of 3.6 K, while the nighttime LST shows an average increase of 2.0 K. Regarding spatial variability, during the mornings the increase in LST is greater in coastal cities (4.1 K); the largest increase in nocturnal LST occurs in inland cities (2.3 K). The smaller increase in LST detected overnight may be due to cooling rates produced by green areas within cities and areas of abundant vegetation that are often found on the outskirts of cities. These values are in line with the increases reported in the cities of Singapore [27] of 3 K or in the city of Seoul [24] of between 3.3 and 4.5 in heat waves. suffered between 2012 and 2016. The greatest increase in LST in coastal cities could be due, in turn, to an increase in ambient temperature caused by the variation in sea breezes. These values, corroborated by statistical analysis, are in line with the results obtained in the USA [21,107], in China [20,21] or in the city of Athens [23,33]. The results in terms of SUHI also indicate significant increases during heat wave periods, with an average value of 2.8 K. The average daytime SUHI of the cities investigated gives an increase of 2.6 K, while the average increase of night SUHI rises to 2.9 K. As for the geographical area, it should be noted that both in the morning and at night the greatest increase in SUHI is detected in the cities of the interior, with average values of 2.8 K and 3.0 K, respectively. These increases are in line with those reported in similar investigations and determine how the intense anticyclonic situation lowers the intensity of the winds and increases radiation, temperature and SUHI [2,23,54,95,97,102,103,106,108].

An increase in ambient temperatures produces warming of the waterproof materials that line buildings and streets. This heat, even after sunset, is emitted by the materials into the atmosphere, hence greater during periods of heat wave than during normal periods. The reason behind a lower intensity of SUHI in coastal cities would be that, at night, the winds from the sea produce a cooling effect in coastal cities. These results were corroborated by means of statistical analysis and again are in line with results reported for the USA [18,22], China [2,21], or Athens [23,33], further validating the results presented here. Our results and establishments are in agreement with some studies [61,109,110] related to heat flux, heat flux storage and how these lead to greater effects or problems in SUHI during the night. Research carried out in the cities of Athens [23], Seoul city [24] or Singapore [27] report these circumstances as fundamental elements in the intensification of SUHI.

5. Conclusions

In recent decades, episodes of high temperatures and heat waves have become more persistent over diverse parts of the planet Earth. In coming decades these exceptional situations will affect larger land surfaces, compounding their social, economic and envi-

ronmental impact. A better knowledge of these conditions is needed in order to establish resilience measures that might improve the climatic conditions of cities.

Our results indicate that environmental pollutants (aerosols, SO_2, NO_2 and CO) increase during periods of heat waves in the cities of southern Spain investigated here. On the contrary, the pollutant O_3 shows a decrease. High temporal and geographical variability of the pollutants analyzed is observed, accentuated in inland cities.

Associated with this increase in pollutants, the LST and SUHI of cities rise during heat wave situations. The average increase for the first variable was 2.8 K and was greater in the morning than in the evening. The largest daytime increase was recorded in coastal cities. However, the highest overnight increase was observed in inland cities, not coastal ones. The mean increase in the SUHI of the surveyed cities, 2.8 K, was greater in the nighttime readings than in the daytime ones. Inland cities suffer the greatest increase in LST during the day and at night; for coastal cities, the increase is smaller.

It is deemed necessary that further research endeavors should increase the number of days of analysis without heat waves versus with a heat wave. This research contemplates just three heat wave periods. New studies should also explore the differences in the nature of heat waves depending on the proximity to the sea. Although some heat transfer can be considered as a return to normal, this is not the case for latent heat transfer. Heat waves generally accompany or induce prolonged periods of extreme dryness that disrupt the water balance of permeable and impervious surfaces. It would be necessary for future studies, to establish the degree of effect of maritime traffic on the pollution of coastal cities. Cities such as Cadiz and Malaga are very close to the Strait of Gibraltar, the passageway for the vast majority of maritime traffic in the Mediterranean Sea.

Our findings here, and in the scope of practice, can form a comprehensive basis that will improve our understanding of heat waves in conjunction with increased environmental pollutants and heightened effects on the LST and SUHI of cities. Studies along these lines should help the persons responsible for city planning when tackling new areas of growth. Minimizing the effects of the LST and SUHI, in view of the geographic situation of the city, calls for implementing efficient and sustainable measures. Key decisions could be made in light of relevant environmental studies such as the ones cited here. Furthermore, our findings could be extrapolated to other Mediterranean cities that share the general characteristics of Andalusia, contributing to future research efforts of this type, especially taking into account that the Sentinel-3 satellite images are available to the entire scientific community.

Supplementary Materials: The following are available online at https://www.mdpi.com/article/10.3390/su141912262/s1, Figure S1. Daytime LST (a) without heat wave (b) with heat wave. Figure S2. Nighttime LST (a) without heat wave (b) with heat wave. Figure S3. SO_2 concentration Sentinel 5P (a) without heat wave (b) with heat wave. Figure S4. NO_2 concentration Sentinel 5P (a) without heat wave (b) with heat wave. Figure S5. CO concentration Sentinel 5P (a) without heat wave (b) with heat wave. Figure S6. Aerosol concentration Sentinel 5P (a) without heat wave (b) with heat wave. Figure S7. O_3 concentration Sentinel 5P (a) without heat wave (b) with heat wave.

Author Contributions: Conceptualization, D.H.G. and J.A.D.; methodology, D.H.G.; software, D.H.G.; validation, D.H.G., J.A.D., A.M.M. and E.G.C.; formal analysis, D.H.G., J.A.D., A.M.M. and E.G.C.; investigation, D.H.G., J.A.D., A.M.M. and E.G.C.; resources, D.H.G., J.A.D., A.M.M. and E.G.C.; data curation, D.H.G.; writing—original draft preparation, D.H.G., J.A.D., A.M.M. and E.G.C.; writing—review and editing, D.H.G., J.A.D., A.M.M. and E.G.C.; visualization, D.H.G., J.A.D., A.M.M. and E.G.C.; supervision, D.H.G., J.A.D., A.M.M. and E.G.C.; project administration, D.H.G., J.A.D., A.M.M. and E.G.C. All authors have read and agreed to the published version of the manuscript.

Funding: This research received no external funding.

Institutional Review Board Statement: Not applicable.

Informed Consent Statement: Not applicable.

Data Availability Statement: In this section, please provide details regarding where data supporting reported results can be found, including links to publicly archived datasets analyzed or generated during the study. Please refer to suggested Data Availability Statements in section "MDPI Research Data Policies" at https://www.mdpi.com/ethics. You might choose to exclude this statement if the study did not report any data.

Conflicts of Interest: The authors declare no conflict of interest.

Abbreviations

AEMET	Meteorology Statal Agency
AOD	Aerosol Optical Depth
AQI	Air Quality Index
BVOCs	Biogenic Volatile Organic Compounds
ESA	European Space Agency
EUROSTAT	European Statistical Office
GLS	Generalized Least Squares
IEM	Intragroup Estimation Method
LST	Land Surface Temperature
MBE	Mean Error Bias
OMS	ordinary squares method
RMSE	Root Mean Square Error
SLSTR	Sean and Land Surface Temperature Radiometer
SUHI	Surface Urban Heat Island
TIRS	Thermal Infrared Sensors
TROPOMI	Tropospheric Monitoring Instrument
UHS	Urban Heat Island
VOCs	Volatile Organic Compounds

References

1. Carvalho, D.; Martins, H.; Marta-Almeida, M.; Rocha, A.; Borrego, C. Urban resilience to future urban heat waves under a climate change scenario: A case study for Porto urban area (Portugal). *Urban Clim.* **2017**, *19*, 1–27. [CrossRef]
2. Jiang, P.; Fu, X.; Fan, Y.; Klemeš, J.; Chen, P.; Ma, S.; Zhang, W. Spatial-temporal potential exposure risk analytics and urban sustainability impacts related to COVID-19 mitigation: A perspective from car mobility behaviour. *J. Clean. Prod.* **2021**, *279*, 123673. [CrossRef] [PubMed]
3. Li, J.; Song, C.; Cao, L.; Zhu, F.; Meng, X.; Wu, J. Impacts of landscape structure on surface urban heat islands: A case study of Shanghai, China. *Remote Sens. Environ.* **2011**, *115*, 3249–3263. [CrossRef]
4. Song, J.; Chen, W.; Zhang, J.; Huang, K.; Hou, B.; Prishchepov, A.V. Effects of building density on land surface temperature in China: Spatial patterns and determinants. *Landsc. Urban Plan.* **2020**, *198*, 103794. [CrossRef]
5. Yang, C.; Yan, F.; Zhang, S. Comparison of land surface and air temperatures for quantifying summer and winter urban heat island in a snow climate city. *J. Environ. Manag.* **2020**, *265*, 110563. [CrossRef] [PubMed]
6. Stewart, I.D.; Oke, T.R. Local climate zones for urban temperature studies. *Bull. Am. Meteorol. Soc.* **2012**, *93*, 1879–1900. [CrossRef]
7. An, N.; Dou, J.; González-Cruz, J.E.; Bornstein, R.D.; Miao, S.; Li, L. An observational case study of synergies between an intense heat wave and the urban heat island in Beijing. *J. Appl. Meteorol. Climatol.* **2020**, *59*, 605–620. [CrossRef]
8. Arnfield, A.J. Two decades of urban climate research: A review of turbulence, exchanges of energy and water, and the urban heat island. *Int. J. Climatol.* **2003**, *23*, 1–26. [CrossRef]
9. Zhou, D.; Zhao, S.; Zhang, L.; Sun, G.; Liu, Y. The footprint of urban heat island effect in China. *Sci. Rep.* **2015**, *5*, 2–12. [CrossRef] [PubMed]
10. Anjos, M.; Targino, A.C.; Krecl, P.; Oukawa, G.Y.; Braga, R.F. Analysis of the urban heat island under different synoptic patterns using local climate zones. *Build. Environ.* **2020**, *185*, 107268. [CrossRef]
11. Luo, M.; Lau, N.C. Increasing Heat Stress in Urban Areas of Eastern China: Acceleration by Urbanization. *Geophys. Res. Lett.* **2018**, *45*, 60–69. [CrossRef]
12. Tewari, M.; Yang, J.; Kusaka, H.; Salamanca, F.; Watson, C.; Treinish, L. Interaction of urban heat islands and heat waves under current and future climate conditions and their mitigation using green and cool roofs in New York City and Phoenix, Arizona. *Environ. Res. Lett.* **2019**, *14*, 034002. [CrossRef]
13. Zhao, L.; Oppenheimer, M.; Zhu, Q.; Baldwin, J.W.; Ebi, K.L.; Bou-Zeid, E.; Guan, K.; Liu, X. Interactions between urban heat islands and heat waves. *Environ. Res. Lett.* **2018**, *13*, 034003. [CrossRef]
14. Huang, F.; Zhan, W.; Wang, Z.H.; Voogt, J.; Hu, L.; Quan, J.; Liu, C.; Zhang, N.; Lai, J. Satellite identification of atmospheric-surface-subsurface urban heat islands under clear sky. *Remote Sens. Environ.* **2020**, *250*, 112039. [CrossRef]

15. Lai, J.; Zhan, W.; Huang, F.; Voogt, J.; Bechtel, B.; Allen, M.; Peng, S.; Hong, F.; Liu, Y.; Du, P. Identification of typical diurnal patterns for clear-sky climatology of surface urban heat islands. *Remote Sens. Environ.* **2018**, *217*, 203–220. [CrossRef]
16. Santamouris, M. Recent progress on urban overheating and heat island research. Integrated assessment of the energy, environmental, vulnerability and health impact. Synergies with the global climate change. *Energy Build.* **2020**, *207*, 109482. [CrossRef]
17. Karimian, H.; Qi, L.; Chen, H. Assessing urban sustainable development in isfahan. *Appl. Mech. Mater.* **2013**, *253*, 244–248. [CrossRef]
18. Li, Z.-L.; Tang, B.-H.; Wu, H.; Ren, H.; Yan, G.; Wan, Z.; Trigo, I.F.; Sobrino, J.A. Satellite-derived land surface temperature: Current status and perspectives. *Remote Sens. Environ.* **2013**, *131*, 14–37. [CrossRef]
19. He, B.J.; Wang, J.; Liu, H.; Ulpiani, G. Localized synergies between heat waves and urban heat islands: Implications on human thermal comfort and urban heat management. *Environ. Res.* **2021**, *193*, 110584. [CrossRef]
20. Jiang, S.; Lee, X.; Wang, J.; Wang, K. Amplified Urban Heat Islands during Heat Wave Periods. *J. Geophys. Res. Atmos.* **2019**, *124*, 7797–7812. [CrossRef]
21. Li, D.; Sun, T.; Liu, M.; Yang, L.; Wang, L.; Gao, Z. Contrasting responses of urban and rural surface energy budgets to heat waves explain synergies between urban heat islands and heat waves. *Environ. Res. Lett.* **2015**, *10*, 054009. [CrossRef]
22. Ramamurthy, P.; Bou-Zeid, E. Heatwaves and urban heat islands: A comparative analysis of multiple cities. *J. Geophys. Res.* **2017**, *122*, 168–178. [CrossRef]
23. Founda, D.; Santamouris, M. Synergies between Urban Heat Island and Heat Waves in Athens (Greece), during an extremely hot summer (2012). *Sci. Rep.* **2017**, *7*, 1–11. [CrossRef] [PubMed]
24. Ngarambe, J.; Nganyiyimana, J.; Kim, I.; Santamouris, M.; Young Yun, G. Synergies between urban heat island and heat waves in Seoul: The role of wind speed and land use characteristics. *PLoS ONE* **2020**, *15*, e0243571. [CrossRef] [PubMed]
25. Richard, Y.; Pohl, B.; Rega, M.; Pergaud, J.; Thevenin, T.; Emery, J.; Dudek, J.; Vairet, T.; Zito, S.; Chateau-Smith, C. Is Urban Heat Island intensity higher during hot spells and heat waves (Dijon, France, 2014–2019)? *Urban Clim.* **2021**, *35*, 100747. [CrossRef]
26. Rizvi, S.H.; Alam, K.; Iqbal, M.J. Spatio-temporal variations in urban heat island and its interaction with heat wave. *J. Atmos. Sol. Terr. Phys.* **2019**, *185*, 50–57. [CrossRef]
27. Chew, L.W.; Liu, X.; Li, X.X.; Norford, L.K. Interaction between heat wave and urban heat island: A case study in a tropical coastal city, Singapore. *Atmos. Res.* **2021**, *247*, 105134. [CrossRef]
28. Rasilla, D.; Allende, F.; Martilli, A.; Fernández, F. Heat waves and human well-being in Madrid (Spain). *Atmosphere* **2019**, *10*, 288. [CrossRef]
29. Qiu, T.; Song, C.; Clark, J.S.; Seyednasrollah, B.; Rathnayaka, N.; Li, J. Understanding the continuous phenological development at daily time step with a Bayesian hierarchical space-time model: Impacts of climate change and extreme weather events. *Remote Sens. Environ.* **2020**, *247*, 111956. [CrossRef]
30. Venter, Z.S.; Brousse, O.; Esau, I.; Meier, F. Hyperlocal mapping of urban air temperature using remote sensing and crowdsourced weather data. *Remote Sens. Environ.* **2020**, *242*, 111791. [CrossRef]
31. Yoon, D.; Cha, D.H.; Lee, G.; Park, C.; Lee, M.I.; Min, K.H. Impacts of Synoptic and Local Factors on Heat Wave Events Over Southeastern Region of Korea in 2015. *J. Geophys. Research. Atmos.* **2018**, *123*, 81–96. [CrossRef]
32. Zhao, L.; Lee, X.; Smith, R.B.; Oleson, K. Strong contributions of local background climate to urban heat islands. *Nature* **2014**, *511*, 216–219. [CrossRef] [PubMed]
33. Founda, D.; Pierros, F.; Petrakis, M.; Zerefos, C. Interdecadal variations and trends of the Urban Heat Island in Athens (Greece) and its response to heat waves. *Atmos. Res.* **2015**, *161*, 1–13. [CrossRef]
34. Basara, J.B.; Basara, H.G.; Illston, B.G.; Crawford, K.C. The Impact of the Urban Heat Island during an Intense Heat Wave in Oklahoma City. *Adv. Meteorol.* **2010**, *2010*, 1–10. [CrossRef]
35. MCGregor, G.R.; Felling, M.; Wolf, T.; Gosling, S. *The Social Impacts of Heat Waves*; Science Report—SC20061/SR6; Environment Agency: Bristol, UK, 2007.
36. House, M.; Santamouris, M. Advances in Building Energy Research Heat Island Research in Europe: The State of Heat Island Research in Europe. *State Art* **2011**, *1*, 37–41. [CrossRef]
37. Ao, X.; Wang, L.; Zhi, X.; Gu, W.; Yang, H.; Li, D. Observed synergies between urban heat islands and heat waves and their controlling factors in Shanghai, China. *J. Appl. Meteorol. Climatol.* **2019**, *58*, 1955–1972. [CrossRef]
38. Andersson, D.; Nässén, J. Should environmentalists be concerned about materialism? An analysis of attitudes, behaviours and greenhouse gas emissions. *J. Environ. Psychol.* **2016**, *48*, 1–11. [CrossRef]
39. Pani, S.K.; Lin, N.H.; RavindraBabu, S. Association of COVID-19 pandemic with meteorological parameters over Singapore. *Sci. Total Environ.* **2020**, *740*, 140112. [CrossRef]
40. Chen, Y.; Li, H.; Karimian, H.; Li, M.; Fan, Q.; Xu, Z. Spatio-temporal variation of ozone pollution risk and its influencing factors in China based on Geodetector and Geospatial models. *Chemosphere* **2022**, *302*, 134843. [CrossRef] [PubMed]
41. Meehl, G.A.; Tebaldi, C. More intense, more frequent, and longer lasting heat waves in the 21st century. *Science* **2004**, *305*, 994–997. [CrossRef]
42. Sun, Y.; Zhang, X.; Zwiers, F.W.; Song, L.; Wan, H.; Hu, T. Rapid increase in the risk of extreme summer heat in Eastern China. *Nat. Clim. Change* **2014**, *4*, 1082–1085. [CrossRef]

43. Coumou, D.; Robinson, A.; Rahmstorf, S. Global increase in record-breaking monthly-mean temperatures. *Clim. Change* **2013**, *118*, 771–782. [CrossRef]
44. Lau, N.C.; Nath, M.J. A model study of heat waves over North America: Meteorological aspects and projections for the twenty-first century. *J. Clim.* **2012**, *25*, 4761–4764. [CrossRef]
45. Valor, E.; Meneu, V.; Caselles, V. Daily air temperature and electricity load in Spain. *J. Appl. Meteorol.* **2001**, *40*, 1413–1421. [CrossRef]
46. Feizizadeh, B.; Blaschke, T. Examining Urban heat Island relations to land use and air pollution: Multiple endmember spectral mixture analysis for thermal remote sensing. *IEEE J. Sel. Top. Appl. Earth Obs. Remote Sens.* **2013**, *6*, 1749–1756. [CrossRef]
47. Poumadère, M.; Mays, C.; Le Mer, S.; Blong, R. The 2003 heat wave in France: Dangerous climate change here and now. *Risk Anal.* **2005**, *25*, 1483–1494. [CrossRef] [PubMed]
48. Semenza, J.; Rubin, C.; Falter, K.; Selanikio, J.; Flanders, W.; Howe, H.; Wilhelm, J. Heat-related deaths during the July 1995 heat wave in Chicago. *N. Engl. J. Med.* **1996**, *335*, 86–90. [CrossRef] [PubMed]
49. Robine, J.M.; Cheung, S.L.K.; Le Roy, S.; Van Oyen, H.; Griffiths, C.; Michel, J.P.; Richard Herrmann, F. Death toll exceeded 70,000 in Europe during the summer of 2003. *Comptes Rendus Biol.* **2008**, *331*, 171–178. [CrossRef] [PubMed]
50. Grumm, R.H. The central European and russian heat event of July-August 2010. *Bull. Am. Meteorol. Soc.* **2011**, *92*, 1285–1296. [CrossRef]
51. Xia, J.; Tu, K.; Yan, Z.; Qi, Y. The super-heat wave in eastern China during July-August 2013: A perspective of climate change. *Int. J. Climatol.* **2016**, *36*, 1291–1298. [CrossRef]
52. Peña-Angulo, D.; Vicente-Serrano, S.M.; Domínguez-Castro, F.; Reig-Gracia, F.; El Kenawy, A. The potential of using climate indices as powerful tools to explain mortality anomalies: An application to mainland Spain. *Environ. Res.* **2021**, *197*, 111203. [CrossRef] [PubMed]
53. United Nations Organization. 2021. Available online: https://news.un.org/es/story/2022/07/1511872 (accessed on 10 September 2022).
54. Siddiqui, A.; Halder, S.; Chauhan, P.; Kumar, P. COVID-19 Pandemic and City-Level Nitrogen Dioxide (NO_2) Reduction for Urban Centres of India. *J. Indian Soc. Remote Sens.* **2020**, *48*, 999–1006. [CrossRef]
55. Hu, Y.; Dai, Z.; Guldmann, J.M. Modeling the impact of 2D/3D urban indicators on the urban heat island over different seasons: A boosted regression tree approach. *J. Environ. Manag.* **2020**, *266*, 110424. [CrossRef] [PubMed]
56. Mandal, I.; Pal, S. COVID-19 pandemic persuaded lockdown effects on environment over stone quarrving and crushing areas. *Sci. Total Environ.* **2020**, *732*, 129281. [CrossRef] [PubMed]
57. Roy, S.; Pandit, S.; Eva, E.A.; Bagmar, M.S.H.; Papia, M.; Banik, L.; Dube, T.; Rahman, F.; Razi, M.A. Examining the nexus between land surface temperature and urban growth in Chattogram Metropolitan Area of Bangladesh using long term Landsat series data. *Urban Clim.* **2020**, *32*, 100593. [CrossRef]
58. Sejati, A.W.; Buchori, I.; Rudiarto, I. The spatio-temporal trends of urban growth and surface urban heat islands over two decades in the Semarang Metropolitan Region. *Sustain. Cities Soc.* **2019**, *46*, 101432. [CrossRef]
59. Shafizadeh-Moghadam, H.; Weng, Q.; Liu, H.; Valavi, R. Modeling the spatial variation of urban land surface temperature in relation to environmental and anthropogenic factors: A case study of Tehran, Iran. *GISci. Remote Sens.* **2020**, *57*, 483–496. [CrossRef]
60. Song, J.; Lin, T.; Li, X.; Prishchepov, A.V. Mapping urban functional zones by integrating very high spatial resolution remote sensing imagery and points of interest: A case study of Xiamen, China. *Remote Sens.* **2018**, *10*, 1737. [CrossRef]
61. Wang, K.; Jiang, S.; Wang, J.; Zhou, C.; Wang, X.; Lee, X. Comparing the diurnal and seasonal variabilities of atmospheric and surface urban heat islands based on the Beijing urban meteorological network. *J. Geophys. Res. Atmos.* **2017**, *122*, 2131–2154. [CrossRef]
62. Sobrino, J.A.; Jiménez-Muñoz, J.C.; Sòria, G.; Ruescas, A.B.; Danne, O.; Brockmann, C.; Ghent, D.; Remedios, J.; North, P.; Merchant, C.; et al. Synergistic use of MERIS and AATSR as a proxy for estimating Land Surface Temperature from Sentinel-3 data. *Remote Sens. Environ.* **2016**, *179*, 149–161. [CrossRef]
63. Mehmood, K.; Bao, Y.; Petropoulos, G.P.; Abbas, R.; Abrar, M.M.; Mustafa, A.; Soban, A.; Saud, S. Investigating connections between COVID-19 pandemic, air pollution and community interventions for Pakistan employing geoinformation technologies. *Chemosphere* **2021**, *272*, 129809. [CrossRef] [PubMed]
64. Sur, K. Variation of tropospheric NO_2 over Indo-Gangetic plain during COVID-19 outbreak in India. *Spat. Inf. Res.* **2021**, *29*, 841–855. [CrossRef]
65. Bar, S.; Parida, B.R.; Mandal, S.P.; Pandey, A.C.; Kumar, N.; Mishra, B. Impacts of COVID-19 lockdown on NO_2 and PM2.5 levels in major urban cities of Europe and USA. *Cities* **2021**, *117*, 103308. [CrossRef]
66. Markham, B.; Barsi, J.; Kvaran, G.; Ong, L.; Kaita, E.; Biggar, S.; Czapla-Myers, J.; Mishra, N.; Helder, D. Landsat-8 operational land imager radiometric calibration and stability. *Remote Sens.* **2014**, *6*, 12275–12308. [CrossRef]
67. Kaplan, G.; Avdan, U.; Avdan, Z.Y. Urban Heat Island Analysis Using the Landsat 8 Satellite Data: A Case Study in Skopje, Macedonia. *Sustainability* **2018**, *2*, 358. [CrossRef]
68. Di Sabatino, S.; Barbano, F.; Brattich, E.; Pulvirenti, B. The multiple-scale nature of urban heat island and its footprint on air quality in real urban environment. *Atmosphere* **2020**, *11*, 1186. [CrossRef]
69. Schaefer, M.; Ebrahimi Salari, H.; Köckler, H.; Thinh, N.X. Assessing local heat stress and air quality with the use of remote sensing and pedestrian perception in urban microclimate simulations. *Sci. Total Environ.* **2021**, *794*, 148709. [CrossRef] [PubMed]

70. De Castro, M.; Gallardo, C.; Jylha, K.; Tuomenvirta, H. The use of a climate-type classification for assessing climate change effects in Europe from an ensemble of nine regional climate models. *Clim. Change* **2007**, *81*, 329–341. [CrossRef]
71. Hidalgo, D. Analysis of synergies between the Urban Heat Island and Heat Waves using Sentinel 3 satellite images: Study of Andalusian cities (Spain). *Earth Syst. Environ.* **2022**, *6*, 199–219. [CrossRef]
72. García, D.H.; Díaz, J.A. Impacts of the COVID-19 confinement on air quality, the Land Surface Temperature and the urban heat island in eight cities of Andalusia (Spain). *Remote Sens. Appl. Soc. Environ.* **2022**, *25*, 100667. [CrossRef]
73. Avdan, U.; Jovanovska, G. Algorithm for automated mapping of land surface temperature using Landsat 8 satellite data. *J. Sens.* **2016**, *16*, 1480307. [CrossRef]
74. Gallo, K.; Hale, R.; Tarpley, D.; Yu, Y. Evaluation of the relationship between air and land surface temperature under clear-and cloudy-sky conditions. *J. Appl. Meteorol. Climatol.* **2011**, *50*, 767–775. [CrossRef]
75. Liu, L.; Zhang, Y. Urban heat island analysis using the landsat TM data and ASTER Data: A case study in Hong Kong. *Remote Sens.* **2011**, *3*, 1535–1552. [CrossRef]
76. Mukherjee, F.; Singh, D. Assessing Land Use—Land Cover Change and Its Impact on Land Surface Temperature Using Landsat Data: A Comparison of Two Urban Areas in India. *Earth Syst. Environ.* **2020**, *4*, 385–407. [CrossRef]
77. Rongali, G.; Keshari, A.K.; Gosain, A.K.; Khosa, R. A mono-window algorithm for land surface temperature estimation from landsat 8 thermal infrared sensor data: A case study of the beas river basin, India. *Pertanika J. Sci. Technol.* **2018**, *26*, 829–840.
78. Alcock, I.; White, M.P.; Lovell, R.; Higgins, S.L.; Osborne, N.J.; Husk, K.; Wheeler, B.W. What accounts for "England's green and pleasant land"? A panel data analysis of mental health and land cover types in rural England. *Landsc. Urban Plan.* **2015**, *142*, 38–46. [CrossRef]
79. Chen, Y.; Li, X.; Zheng, Y.; Guan, Y.; Liu, X. Estimating the relationship between urban forms and energy consumption: A case study in the Pearl River Delta, 2005–2008. *Landsc. Urban Plan.* **2011**, *102*, 33–42. [CrossRef]
80. Fang, L.; Tian, C. Construction land quotas as a tool for managing urban expansion. *Landsc. Urban Plan.* **2020**, *195*, 103727. [CrossRef]
81. McMillin, L.M. Estimation of sea surface temperatures from two infrared window measurements with different absorption. *J. Geophys. Res.* **1975**, *80*, 5113–5117. [CrossRef]
82. Ruescas Orient, A.; Quereda Sala, J.; Montón Chiva, E.; Escrig Barberá, J.; Mollá Cantavella, B. La detección del efecto térmico urbano a través de las imágenes NOAA. *Cuad. De Geogr.* **2003**, *73*, 343–362. [CrossRef]
83. Pérez González, M.E.; García Rodríguez, M.P.; Guerra Zeballos, A. Análisis del clima urbano a partir de imágenes de satélite en el centro peninsular español. *An. De Geograía De La Univ. Complut.* **2003**, *23*, 187–206.
84. Remedios, J.; Emsley, S. Sentinel-3 Optical Products and Algorithm Definition Land Surface Temperature. Reference S3-L2-SD-03-T03-ULNILU-ATBD, 2012. Available online: https://sentinel.esa.int/documents/247904/349589/SLSTR_Level-2_LST_ATBD.pdf (accessed on 24 August 2022).
85. Yang, J.; Zhou, J.; Göttsche, F.-M.; Long, Z.; Ma, J.; Luo, R. Investigation and validation of algorithms for estimating land surface temperature from Sentinel-3 SLSTR data. *Int. J. Appl. Earth Obs. Geoinf.* **2020**, *91*, 102136. [CrossRef]
86. Oke, T.R. *Boundary Layer Climates*; Routledge: London, UK, 1987.
87. Wang, L.; Lu, Y.; Yao, Y. Comparison of three algorithms for the retrieval of land surface temperature from landsat 8 images. *Sensors* **2019**, *19*, 5049. [CrossRef] [PubMed]
88. Labra, R. *Zero Panel Data Guide*; Cátedra UA: Madrid, Spain, 2014; pp. 1–61. Available online: https://www.catedrauam-asseco.com/documents/Working%20papers/WP2014_16_Guia%20CERO%20para%20datos%20de%20panel_Un%20enfoque%20practico.pdf (accessed on 26 September 2022).
89. Seto, K.C.; Kaufmann, R.K. Modeling the drivers of urban land use change in the Pearl River Delta, China: Integrating remote sensing with socioeconomic data. *Land Econ.* **2003**, *79*, 106–121. [CrossRef]
90. Li, D.; Bou-Zeid, E. Synergistic interactions between urban heat islands and heat waves: The impact in cities is larger than the sum of its parts. *J. Appl. Meteorol. Climatol.* **2013**, *52*, 2051–2064. [CrossRef]
91. Ackerman, S.A.; Knox, J. *Meteorology: Understanding the Atmosphere*; Jones and Bartlett Learning: Burlington, MA, USA, 2012; p. 578.
92. Russo, A.; Sousa, P.M.; Durão, R.M.; Ramos, A.M.; Salvador, P.; Linares, C.; Díaz, J.; Trigo, R.M. Saharan dust intrusions in the Iberian Peninsula: Predominant synoptic conditions. *Sci. Total Environ.* **2020**, *717*, 137041. [CrossRef] [PubMed]
93. Xoplaki, E.; González-Rouco, J.F.; Gyalistras, D.; Luterbacher, J.; Rickli, R.; Wanner, H. Interannual summer air temperature variability over Greece and its connection to the large-scale atmospheric circulation and Mediterranean SSTs 1950–1999. *Clim. Dyn.* **2003**, *20*, 537–554. [CrossRef]
94. Sousa, P.M.; Barriopedro, D.; Ramos, A.M.; García-Herrera, R.; Espírito-Santo, F.; Trigo, R.M. Saharan air intrusions as a relevant mechanism for Iberian heatwaves: The record breaking events of August 2018 and June 2019. *Weather. Clim. Extrem.* **2019**, *26*, 100224. [CrossRef]
95. Fischer, P.H.; Brunekreef, B.; Lebret, E. Air pollution related deaths during the 2003 heat wave in the Netherlands. *Atmos. Environ.* **2004**, *38*, 1083–1085. [CrossRef]
96. Hoffmann, W.; Terschu, C.; Udke-dost, K. Measurements of Extremely Frequency Electromagnetic Fields (50 Hz) in Private Homes in Germany—Results of a Representative Sample of N = 1935. *Epidemiology* **2004**, *15*, 115–133. [CrossRef]
97. Ordóñez, C.; Elguindi, N.; Stein, O.; Huijnen, V.; Flemming, J.; Inness, A.; Flentje, H.; Katragkou, E.; Moinat, P.; Peuch, V.-H.; et al. Global model simulations of air pollution during the 2003 European heat wave. *Atmos. Chem. Phys.* **2010**, *10*, 789–815. [CrossRef]

98. Shaposhnikov, D.; Revich, B.; Bellander, T.; Bedada, G.B.; Bottai, M.; Kharkova, T.; Kvasha, E.; Lezina, E.; Lind, T.; Semutnikovaet, E.; et al. Mortality related to air pollution with the Moscow heat wave and wildfire of 2010. *Epidemiology* **2014**, *25*, 359–364. [CrossRef] [PubMed]
99. Zhao, F.; Liu, C.; Cai, Z.; Liu, X.; Bak, J.; Kim, J. Ozone profile retrievals from TROPOMI: Implication for the variation of tropospheric ozone during the outbreak of COVID-19 in China. *Sci. Total Environ.* **2021**, *764*, 142886. [CrossRef]
100. Zou, Y.; Charlesworth, E.; Yin, C.Q.; Yan, X.L.; Deng, X.J.; Li, F. The weekday/weekend ozone differences induced by the emissions change during summer and autumn in Guangzhou, China. *Atmos. Environ.* **2019**, *199*, 114–126. [CrossRef]
101. Karimian, H.; Li, Q.; Li, C.; Chen, G.; Mo, Y.; Wu, C.; Fan, J. Spatio-temporal variation of wind influence on distribution of fine particulate matter and its precursor gases. *Atmos. Pollut. Res.* **2019**, *10*, 53–64. [CrossRef]
102. Das, N.; Sutradhar, S.; Ghosh, R.; Mondal, P. Asymmetric nexus between air quality index and nationwide lockdown for COVID-19 pandemic in a part of Kolkata metropolitan, India. *Urban Clim.* **2021**, *36*, 100789. [CrossRef]
103. Srivastava, A.K.; Bhoyar, P.D.; Kanawade, V.P.; Devara, P.C.S.; Thomas, A.; Soni, V.K. Improved air quality during COVID-19 at an urban megacity over the Indo-Gangetic Basin: From stringent to relaxed lockdown phases. *Urban Clim.* **2021**, *36*, 100791. [CrossRef] [PubMed]
104. Velasco, E. Impact of Singapore's COVID-19 confinement on atmospheric CO_2 fluxes at neighborhood scale. *Urban Clim.* **2021**, *37*, 100822. [CrossRef] [PubMed]
105. Ghosh, S.; Das, A.; Hembram, T.K.; Saha, S.; Pradhan, B.; Alamri, A.M. Impact of COVID-19 induced lockdown on environmental quality in four Indian megacities Using Landsat 8 OLI and TIRS-derived data and Mamdani fuzzy logic modelling approach. *Sustainability* **2020**, *12*, 5464. [CrossRef]
106. Alqasemi, A.S.; Hereher, M.E.; Kaplan, G.; Al-Quraishi, A.M.F.; Saibi, H. Impact of COVID-19 lockdown upon the air quality and surface urban heat island intensity over the United Arab Emirates. *Sci. Total Environ.* **2021**, *767*, 144330. [CrossRef] [PubMed]
107. Li, T.; Meng, Q. A mixture emissivity analysis method for urban land surface temperature retrieval from Landsat 8 data. *Landsc. Urban Plan.* **2018**, *179*, 63–71. [CrossRef]
108. Toro, R.; Catalán, F.; Urdanivia, F.R.; Rojas, J.P.; Manzano, C.A.; Seguel, R.; Gallardo, L.; Osses, M.; Pantoja, N.; Leiva-Guzman, M.A. Air pollution and COVID-19 lockdown in a large South American city: Santiago Metropolitan Area, Chile. *Urban Clim.* **2021**, *36*, 100803. [CrossRef] [PubMed]
109. Agathangelidis, I.; Cartalis, C.; Santamouris, M. Integrating Urban Form, Function, and Energy Fluxes. *Climate* **2019**, *7*, 75. [CrossRef]
110. Dudorova, N.V.; Belan, B.D. The Energy Model of Urban Heat Island. *Atmosphere* **2022**, *13*, 457. [CrossRef]